Phagocytosis and self-destruction break down dendrites of *Drosophila* sensory neurons at distinct steps of Wallerian degeneration

Hui Ji[a,b,1], Maria L. Sapar[a,b,1,2], Ankita Sarkar[a,b,3], Bei Wang[a,b], and Chun Han[a,b,4]

[a]Weill Institute for Cell and Molecular Biology, Cornell University, Ithaca, NY 14853; and [b]Department of Molecular Biology and Genetics, Cornell University, Ithaca, NY 14853

Edited by Liqun Luo, Department of Biology, Stanford University, Stanford, CA; received June 25, 2021; accepted December 1, 2021

After injury, severed dendrites and axons expose the "eat-me" signal phosphatidylserine (PS) on their surface while they break down. The degeneration of injured axons is controlled by a conserved Wallerian degeneration (WD) pathway, which is thought to activate neurite self-destruction through Sarm-mediated nicotinamide adenine dinucleotide (NAD^+) depletion. While neurite PS exposure is known to be affected by genetic manipulations of NAD^+, how the WD pathway coordinates both neurite PS exposure and self-destruction and whether PS-induced phagocytosis contributes to neurite breakdown in vivo remain unknown. Here, we show that in *Drosophila* sensory dendrites, PS exposure and self-destruction are two sequential steps of WD resulting from Sarm activation. Surprisingly, phagocytosis is the main driver of dendrite degeneration induced by both genetic NAD^+ disruptions and injury. However, unlike neuronal *Nmnat* loss, which triggers PS exposure only and results in phagocytosis-dependent dendrite degeneration, injury activates both PS exposure and self-destruction as two redundant means of dendrite degeneration. Furthermore, the axon-death factor Axed is only partially required for self-destruction of injured dendrites, acting in parallel with PS-induced phagocytosis. Lastly, injured dendrites exhibit a unique rhythmic calcium-flashing that correlates with WD. Therefore, both NAD^+-related general mechanisms and dendrite-specific programs govern PS exposure and self-destruction in injury-induced dendrite degeneration in vivo.

phosphatidylserine | PS exposure | phagocytosis | Wallerian degeneration | dendrite degeneration

Physical insults to the nervous system often disrupt neuronal connectivity and function by damaging dendritic or axonal processes of neurons. Injured axons break down through a series of stereotypical events collectively called Wallerian degeneration (WD) (1, 2). Dendrites undergo a similar program of degeneration after injury (AI) (3). Before neurons can regenerate their processes and restore connections, the debris from damaged neurites has to be promptly cleared by phagocytes, which are cells that engulf dead cells or cell debris (4). Inefficient clearance can lead to neuroinflammation and further exacerbate the damage to the surrounding tissues (5, 6). Although WD is mainly considered to be a neurite-intrinsic, self-destructive process (7), whether phagocytosis actively contributes to degeneration of injured neurites in vivo, rather than merely passively removing neuronal debris, remains unclear.

WD is governed by an evolutionarily conserved pathway, which is also called "axon-death" pathway, because it was discovered in studies focused primarily on axon degeneration in *Drosophila* and rodents (4, 7). In this pathway, injury induces activation of the E3 ubiquitin ligase Highwire/Phr1 in severed axons (8, 9), which in turn causes degradation of nicotinamide mononucleotide adenyltransferase (Nmnat), an enzyme required for the synthesis of nicotinamide adenine dinucleotide (NAD^+) (10). The decrease of NAD^+ resulting from Nmnat degradation (11), together with an accumulation of the NAD^+ precursor nicotinamide mononucleotide (NMN) (12, 13), activates Sarm/SARM1, a sterile alpha/Armadillo/Toll-Interleukin receptor homology domain protein (14–19). Due to its NADase activity, Sarm/SARM1 is thought to subsequently cause local NAD^+ depletion in injured axons (20, 21). In *Drosophila*, *axundead* (*axed*) is required downstream of Sarm for axon degeneration of olfactory receptor neurons and wing sensory neurons (22). The loss of *axed* blocks axon degeneration even when Sarm is dominantly activated, suggesting that Axed activation is a key switch of WD (22). In addition, *pebbled* (*peb*) encodes a *Drosophila* transcription factor required for axon degeneration of glutamatergic but not cholinergic sensory neurons in the wing (23). Although how exactly Axed and/or NAD^+ depletion lead to axon breakdown is still mysterious, it is generally believed that Sarm activity initiates a neurite-intrinsic self-destruction program that ultimately is responsible for WD of axons (7, 9, 21, 22). While the WD pathway is primarily characterized in axons, evidence suggests that NAD^+ reduction is also an essential step in

Significance

Mutations in the nicotinamide adenine dinucleotide (NAD^+) biosynthesis pathway are associated with progressive neurodegeneration; neuronal injury causes rapid breakdown of damaged axons and dendrites. NAD^+ reduction is thought to underlie both types of degeneration by inducing neuronal self-destruction. Here, we show that phagocytosis, instead of self-destruction, drives degeneration of *Drosophila* sensory dendrites in both injury and genetic NAD^+ disruptions. Mechanistically, phagocytosis is induced earlier than self-destruction by these manipulations, as a result of phosphatidylserine exposure on the dendrite surface. In addition, injured dendrites exhibit unique calcium dynamics and only partially require the axon-death factor Axed for self-destruction. Thus, our results suggest important contributions of phagocytosis to NAD^+-related neurodegenerative diseases and highlight the difference between dendrite and axon degeneration.

Author contributions: H.J., M.L.S., and C.H. designed research; H.J., M.L.S., A.S., and B.W. performed research; H.J., M.L.S., A.S., B.W., and C.H. contributed new reagents/analytic tools; H.J., M.L.S., and A.S. analyzed data; and H.J., M.L.S., A.S., and C.H. wrote the paper.

The authors declare no competing interest.

This article is a PNAS Direct Submission.

[1]H.J. and M.L.S. contributed equally to this work.

[2]Present address: The New York Stem Cell Foundation Research Institute, New York, NY 10019.

[3]Present address: Rheonix, Inc., Ithaca, NY 14850.

[4]To whom correspondence may be addressed. Email: chun.han@cornell.edu.

This article contains supporting information online at http://www.pnas.org/lookup/suppl/doi:10.1073/pnas.2111818119/-/DCSupplemental.

Published January 20, 2022.

injury-induced dendrite degeneration (3, 24). However, which components of the WD pathway are conserved in dendrites remains unknown.

Neuronal debris is recognized by resident phagocytes of the nervous system through specific "eat-me" signals exposed on the neuronal surface. A highly conserved eat-me signal is phosphatidylserine (PS), a negatively charged phospholipid normally found in the inner leaflet of the plasma membrane of healthy cells. During apoptosis, PS is externalized to the outer leaflet of the plasma membrane to mark the cell for engulfment (25). Genetic analyses of certain PS-binding bridging molecules and cell membrane receptors in mice and zebrafish suggest that PS recognition contributes to the phagocytosis of neurons (26–28). Similarly, clearance of injured axons and dendrites in *Drosophila* requires Draper (Drpr), an engulfment receptor that binds to PS (8, 29–31). PS exposure has also been directly observed on injured axons of mouse neurons in vitro (32, 33) and on injured dendrites of *Drosophila* sensory neurons in vivo (24). Although axonal PS exposure can be induced independently of axon degeneration in vitro (32), ectopically induced PS exposure resulted in engulfment-dependent neurite reduction of otherwise healthy neurons in both the central nervous system and the peripheral nervous system (PNS) of *Drosophila* (24), pointing to a dominant effect of PS exposure in inducing phagocytosis. Recent studies revealed a link between neuronal PS exposure and the WD pathway. Overexpression (OE) of Wld^S, a fusion protein containing the full-length murine Nmnat1 (34), in *Drosophila* sensory neurons suppresses PS exposure of injured dendrites (24). In addition, *Sarm1* ablation and NAD^+ supplementation in neuronal culture reduce PS exposure on injured axons (32). These observations raise two important questions: How does the WD pathway regulate and coordinate both neurite PS exposure and self-destruction? What are the relative contributions of PS-mediated phagocytosis and neurite self-destruction in WD in vivo?

To address these questions, we utilized *Drosophila* class IV dendritic arborization (C4da) neurons on the larval body wall, an established in vivo model of injury-induced dendrite degeneration (30). In this system, degenerating dendrites of C4da neurons are phagocytosed by epidermal cells through the engulfment receptor Drpr. Here, we show that PS exposure and dendrite self-destruction are two distinct steps downstream of Sarm activation and that in vivo, phagocytosis is the main driving force of dendrite degeneration induced by injury and *Nmnat* loss-of-function (LOF). Furthermore, unlike in axons, Axed is not required for dendrite degeneration: it contributes to injury-induced dendrite self-destruction but is not involved in dendrite PS exposure. Lastly, dendrite degenerations induced by injury and *Nmnat* LOF differ in phagocytosis dependency, membrane disruption, and dendrite calcium dynamics. Injured dendrites exhibit a unique rhythmic calcium-flashing, which is disrupted by Wld^S OE and *axed* loss, indicating a potential role of calcium-flashing in dendrite self-destruction.

Results

***Nmnat* Knockout Induces Sarm-Dependent, Spontaneous Dendrite Degeneration.** To understand how the WD pathway regulates neuronal PS exposure, we first investigated the impact of removing *Nmnat* from C4da neurons. *Nmnat* LOF is known to induce degeneration of eye photoreceptors (35) and wing sensory neurons (22). However, a previous study found that C4da neurons mutant for *Nmnat* did not show dendrite degeneration, despite displaying dendrite reduction and axon degeneration (36). To reexamine the LOF phenotype of *Nmnat*, we used CRISPR-mediated tissue-restricted mutagenesis (CRISPR-TRiM), a tissue-specific mutagenesis method that we previously developed (37), to knock out *Nmnat* in C4da neurons. In this method, *Nmnat* is knocked out by C4da-specific *ppk-Cas9* and two ubiquitously expressed guide RNAs (gRNAs) targeting *Nmnat*. To distinguish dendrite reduction caused by degeneration from that caused by growth defects, we used CD4-tdTomato (CD4-tdTom) to label C4da dendrites. Because tdTom is stable in phagosomes, the presence of tdTom-labeled dendrite debris in epidermal cells is an indication of dendrite breakdown and subsequent engulfment (30).

As expected, *Nmnat* knockout (KO) in C4da neurons (Fig. 1*B*) caused strong dendritic reduction (Fig. 1*G*) in wandering third instar larvae as compared to the control (Fig. 1*A*). In addition, dendrite debris was observed to spread in epidermal cells underneath and near the dendrites of *Nmnat* KO neurons (Fig. 1 *B* and *H*), suggesting that some dendrites had degenerated and were engulfed by epidermal cells. Unlike degenerating dendrites observed during developmental pruning or AI (30, 38), the remaining dendrites of *Nmnat* KO neurons did not show obvious blebbing or fragmentation, which may explain why dendrite degeneration was not detected previously in *Nmnat* mutant C4da neurons, considering that the membrane green fluorescent protein (GFP) marker used to label dendrites in the previous study is rapidly degraded by epidermal cells once engulfed and thus cannot visualize phagosomes (30, 36).

Nmnat protects neurons by both synthesizing NAD^+ and functioning as a chaperone protein (39). To verify that the observed dendrite degeneration is due to the loss of Nmnat enzymatic activity, we tried to rescue *Nmnat* KO neurons by overexpressing Wld^S, which contains full NMNAT activity (34), and $Wld^{S\text{-}dead}$, a mutant version of Wld^S that cannot synthesize NAD^+ but maintains the chaperone function (40). Wld^S OE rescued the degeneration of *Nmnat* KO neurons and restored dendrite morphology to the wild-type level (Fig. 1 *C*, *G*, and *H*), while $Wld^{S\text{-}dead}$ OE did not change dendrite length or debris level of *Nmnat* KO neurons (Fig. 1 *D*, *G*, and *H*). These results suggest that NAD^+ reduction is likely responsible for the dendrite degeneration of *Nmnat* KO neurons.

We next asked whether Sarm plays a role in *Nmnat* KO-induced dendrite degeneration. Indeed, *Sarm* LOF completely blocked dendrite degeneration of *Nmnat* KO neurons (Fig. 1 *F–H*), as evident in the absence of dendrite debris in epidermal cells, even though these neurons showed more variable dendrite length (Fig. 1*G*) compared to *Sarm* LOF alone (Fig. 1 *E*, *G*, and *H*). Importantly, these results demonstrate that *Sarm* is required for the dendrite degeneration of *Nmnat* KO neurons, which is consistent with previous reports that *Sarm1* KO rescued axon outgrowth defects and degeneration associated with *NMNAT2* deficiency in mice (41, 42). All the results above together suggest that *Nmnat* LOF in neurons cause spontaneous dendrite degeneration through Sarm activity.

PS Exposure–Mediated Phagocytosis Causes Dendrite Degeneration of *Nmnat* KO Neurons. To ask whether *Nmnat* KO also causes neuronal PS exposure, we used an established method to visualize PS exposure on C4da dendrites. In this method, the fluorescent PS sensor GFP-Lact is expressed by the larval fat body and secreted into the hemolymph (24). As C4da dendrites are largely exposed to the hemolymph, GFP-Lact labeling allows visualization of dynamic PS exposure on dendrites in intact live animals (24). We found that GFP-Lact strongly labeled *Nmnat* KO neurons at distal branches that underwent degeneration (Fig. 2*B*), while wild-type C4da neurons showed no labeling (Fig. 2*A*). Interestingly, we also observed weaker GFP-Lact labeling on dendrite segments that did not display obvious signs of degeneration (outlined in Fig. 2*B*), suggesting that PS exposure may precede dendrite breakdown, instead of being merely a consequence of dendrite degeneration. This conclusion was further corroborated by time-lapse imaging of *Nmnat* KO neurons (Movie S1) and kymograph analysis (Fig. 2*C*): PS

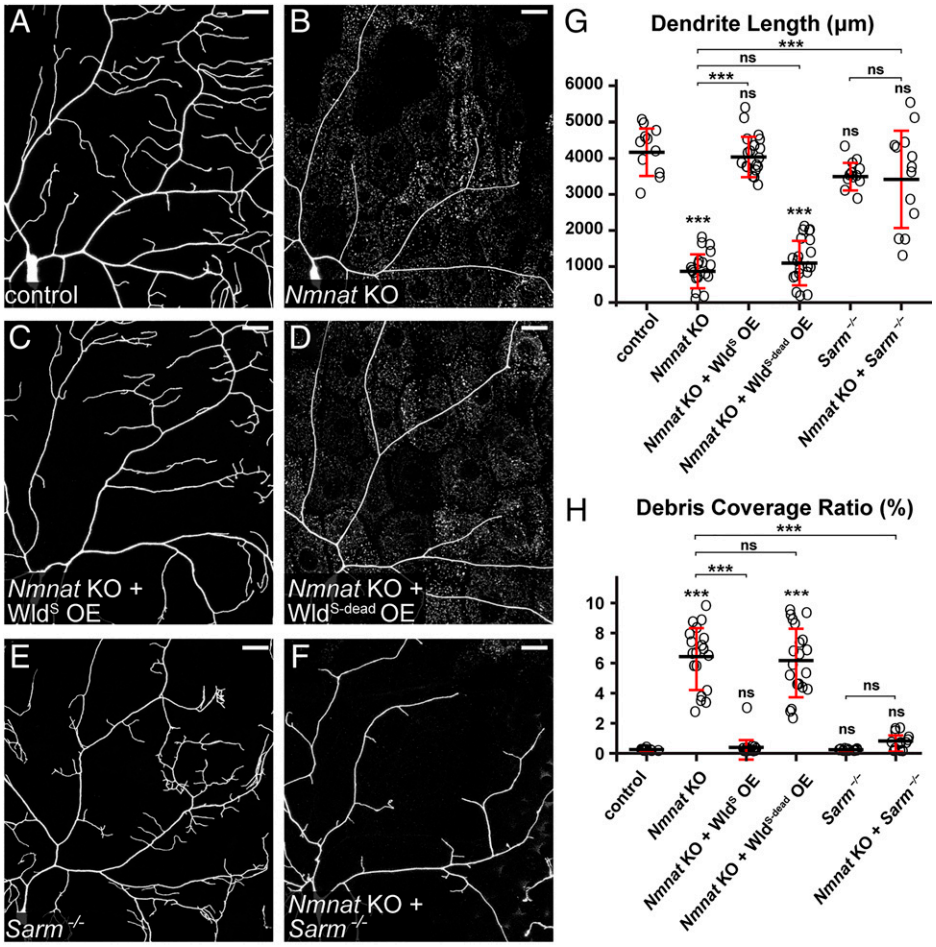

Fig. 1. *Nmnat* KO induces Sarm-dependent, spontaneous dendrite degeneration. (*A*–*F*) Partial dendritic fields of control (*A*), *Nmnat* KO (*B*), *Nmnat* KO + Wld^S OE (*C*), *Nmnat* KO + $Wld^{S\text{-dead}}$ OE (*D*), $Sarm^{4705/4621}$ (*E*), and *Nmnat* KO + $Sarm^{4705/4621}$ (*F*) ddaC C4da neurons. Neurons were labeled by *ppk* > *CD4-tdTom* (*A*–*D*) and *ppk-CD4-tdTom* (*E* and *F*). The C4da-specific KO was induced by *ppk-Cas9*. (Scale bars, 25 μm.) (*G*) Quantification of dendrite length. *n* = number of neurons: control (*n* = 11, six animals); *Nmnat* KO (*n* = 19, 10 animals); *Nmnat* KO + Wld^S OE (*n* = 17, 10 animals); *Nmnat* KO + $Wld^{S\text{-dead}}$ OE (*n* = 20, 11 animals); $Sarm^{4705/4621}$ (*n* = 12, six animals); and *Nmnat* KO + $Sarm^{4705/4621}$ (*n* = 13, eight animals) (one-way ANOVA and Tukey's test). (*H*) Quantification of debris coverage ratio, which is the percentage of debris area normalized by dendrite area ratio. Number of neurons is the same as in *G*. Kruskal–Wallis (one-way ANOVA on ranks) and Dunn's test; *P* values were adjusted with the Benjamini–Hochberg method. For all quantifications, ***$P \leq 0.001$ and ns, not significant. The significance level above each genotype is for comparison with the control. Black bar, mean; red bar, SD.

exposure (indicated by white dotted lines) occurred well ahead of dendrite fragmentation (indicated by blue dotted lines).

As *Sarm* is required for dendrite degeneration of *Nmnat* KO neurons, we asked whether Sarm also regulates PS exposure in these neurons. *Nmnat* KO neurons showed no PS exposure in the *Sarm* mutant background (Fig. 2*D*), suggesting that Sarm activity is also responsible for inducing the observed PS exposure.

The observation of PS exposure on *Nmnat* KO dendrites raises the question of whether PS exposure contributes to dendrite breakdown by inducing phagocytic attacks from epidermal cells. Because PS-mediated epidermal engulfment of dendrites requires Drpr (24), we examined *Nmnat* KO dendrites in *drpr* mutant larvae. Strikingly, *drpr* LOF completely blocked dendrite degeneration of *Nmnat* KO neurons (Fig. 2*H* as compared to *E*–*G* and *J* and *K*). These dendrites exhibited dynamic extension and retraction behaviors (Fig. 2*L* and Movie S2), demonstrating that they were not fragmented dendrites that failed to be cleared. Next, to examine whether dendrite breakdown induced by *Nmnat* KO depends on PS exposure, we tried to rescue *Nmnat* KO neurons by overexpressing ATP8A. ATP8A is the *Drosophila* ortholog of PS flippase responsible for keeping PS in the inner leaflet of the plasma membrane (43, 44), whose LOF in da neurons causes dendritic PS exposure (24). Indeed, ATP8A OE completely blocked dendrite degeneration of *Nmnat* KO neurons and resulted in even less dendrite debris than the wild-type control (Fig. 2 *I* and *K*).

Thus, these data demonstrate that Sarm activity causes dendrite PS exposure, which in turn induces phagocytic attack to drive dendrite degeneration of *Nmnat* KO neurons.

Wld^S OE and *Sarm* KO Suppress PS Exposure and Fragmentation of Injured Dendrites. Wld^S protects injured neurites from degenerating by maintaining the NAD^+ level in the neurites. We previously found that overexpressing Wld^S in C4da neurons blocked fragmentation and PS exposure of ablated dendrites at 10 h AI (24). To further investigate the role of the WD pathway in neuronal PS exposure, we examined the effects of overexpressing Wld^S and knocking out *Sarm* in C4da neurons at 24 h after laser-severing of dendrites. Neuronal-specific KO was conducted using *SOP-Cas9*, which is active in precursor cells of C4da neurons, to minimize potential gene perdurance (37). As expected, Wld^S OE blocked degeneration and clearance of injured dendrites also at 24 h AI (Fig. 3*C*, as compared to the control in Fig. 3*B*), even though the injured arbors were greatly simplified as compared to uninjured dendrites (Fig. 3 *A* and *E*).

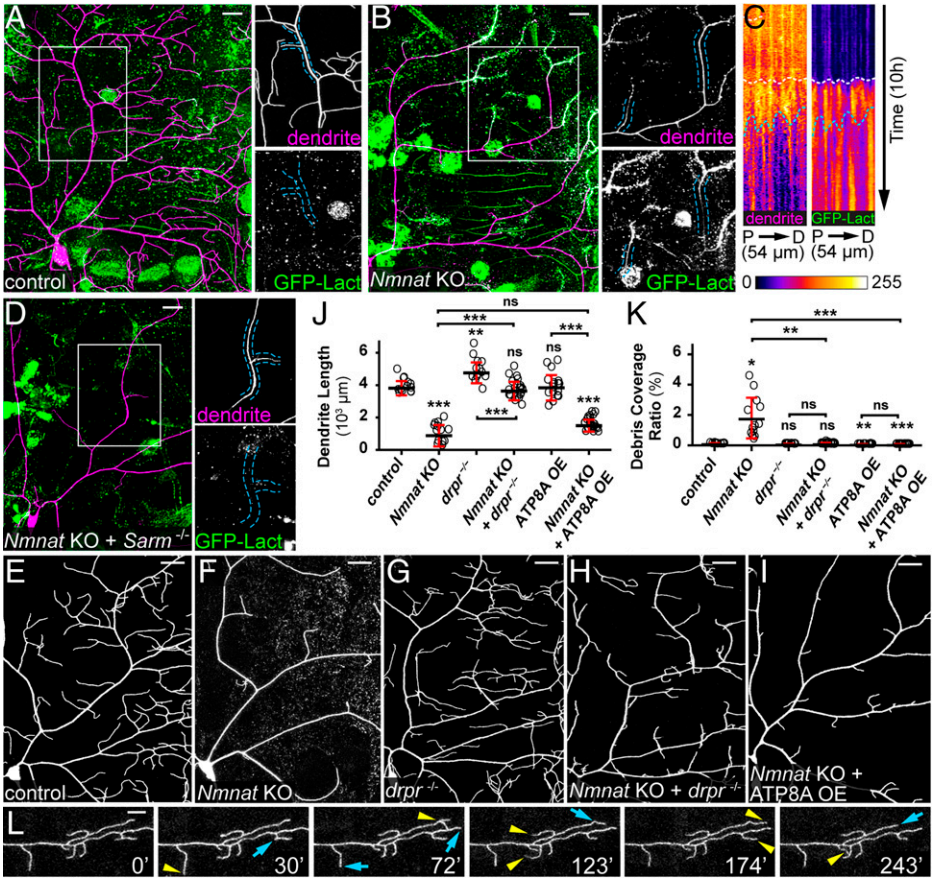

Fig. 2. PS exposure–mediated phagocytosis causes dendrite degeneration of *Nmnat* KO neurons. (*A*) A control ddaC neuron showing the lack of GFP-Lact labeling. *Insets* show close-ups of an intact dendrite. (Scale bar, 25 μm.) (*B*) A *Nmnat* KO ddaC neuron undergoing spontaneous degeneration and showing labeling by GFP-Lact. In the *Inset*, the outlined dendrite segments do not show obvious blebbing or fragmentation but are weakly labeled by GFP-Lact. (Scale bar, 25 μm.) (*C*) Kymographs of dendrite signal (CD4-tdTom, *Left*) and GFP-Lact binding (*Right*) along a dendrite segment of a *Nmnat* KO ddaC neuron over time. For each kymograph panel, the *x*-axis corresponds to the straightened dendrite segment from the proximal (P) to the distal (D) end; the *y*-axis corresponds to time, with each row of pixels representing the maximum intensity along the dendrite in one frame. The total length of the dendrite and the total time are indicated. White dotted lines indicate the timing of GFP-Lact initial binding to the dendrite; blue dotted lines indicate the timing of the dendrite fragmentation based on the continuity of the dendrite signal (Movie S1). (*D*) Dendrites of a *Nmnat* KO + *Sarm*$^{4705/4621}$ ddaC neuron showing the lack of GFP-Lact labeling. *Insets* show close-ups of an intact dendrite. (Scale bar, 25 μm.) (*E–I*) Partial dendritic fields of control (*E*), *Nmnat* KO (*F*), *drpr*$^{-/-}$ (*G*), *Nmnat* KO + *drpr*$^{-/-}$ (*H*), and *Nmnat* KO + ATP8A OE (*I*) neurons. (Scale bars, 25 μm.) (*J*) Quantification of dendrite length. *n* = number of neurons: control (*n* = 13, seven animals); *Nmnat* KO (*n* = 13, seven animals); *drpr*$^{-/-}$ (*n* = 14, eight animals); *Nmnat* KO + *drpr*$^{-/-}$ (*n* = 22, 14 animals); ATP8A OE (*n* = 17, nine animals); and *Nmnat* KO + ATP8A OE (*n* = 23, nine animals) (one-way ANOVA and Tukey's test). (*K*) Quantification of debris coverage ratio. Number of neurons is the same as in *J*. Kruskal–Wallis (one-way ANOVA on ranks) and Dunn's test; *P* values adjusted with the Benjamini–Hochberg method. (*L*) A time series of *Nmnat* KO + *drpr*$^{-/-}$ dendrites. Yellow arrowheads indicate growth of dendrites compared to the previous frame; blue arrows indicate retractions of dendrites compared to the previous frame (Movie S2). (Scale bar, 10 μm.) In all panels, neurons were labeled by *ppk-CD4-tdTom* (*A–H*) and *ppk-MApHS* (*I*). C4da-specific KO was induced by *ppk-Cas9*. For all quantifications, $*P \leq 0.05$, $**P \leq 0.01$, $***P \leq 0.001$, and ns, not significant. The significance level above each genotype is for comparison with the control. Black bar, mean; red bar, SD.

Neuronal-specific *Sarm* KO showed similar effects in injured dendrites (Fig. 3 *D* and *E*) to those of Wld^S OE.

We next examined the effects of Wld^S OE and *Sarm* KO on dendritic PS exposure. While injured dendrites of wild-type neurons robustly exposed PS at 5 h AI (*SI Appendix*, Fig. S1*A*) (24), Wld^S OE prevented PS exposure on severed dendrites as late as 24 h AI, even on branches that showed blebbing and breakage (Fig. 3 *F* and *I*). *Sarm* KO also effectively blocked PS exposure on injured dendrites at 24 h AI (Fig. 3 *G* and *I*), with occasionally strong PS labeling on fragmented distal terminal branches (Fig. 3 *H* and *I*). The above data in dendrite injury together show that Nmnat activity and *Sarm* LOF suppress both PS exposure and degeneration of injured dendrites, likely by preventing NAD^+ depletion.

Ectopic PS Exposure Causes Injured Dendrites of Wld^S OE and *Sarm* KO Neurons to Degenerate. The absence of PS exposure on injured dendrites of Wld^S OE and *Sarm* KO neurons raises the question of whether the degeneration defects of these neurons are due to the lack of PS-mediated phagocytosis by epidermal cells. To test this hypothesis, we ectopically induced neuronal PS exposure by knocking out *CDC50*, which encodes a chaperone necessary for the function of *Drosophila* flippases (43), and by overexpressing TMEM16F, a mammalian PS scramblase (45). These manipulations in C4da neurons cause mild but appreciable phagocytosis-dependent dendrite loss (24). TMEM16F OE and *CDC50* KO each restored PS exposure on injured dendrites of Wld^S OE neurons at 6 to 7 h AI (*SI Appendix*, Fig. S2 *A* and *B*, respectively). These injured dendrites either partially or completely degenerated and were engulfed by epidermal cells by 24 h AI (Fig. 4 *A*, *B*, and *E*). A much-stronger effect was observed when *CDC50* KO and TMEM16F OE were combined in Wld^S OE neurons: degeneration and clearance of injured dendrites were restored to the wild-type level (Fig. 4 *C* and *E*). Similarly, *CDC50* KO and TMEM16F OE caused injured dendrites of *Sarm* KO neurons to completely degenerate (Fig. 4 *D* and *E*).

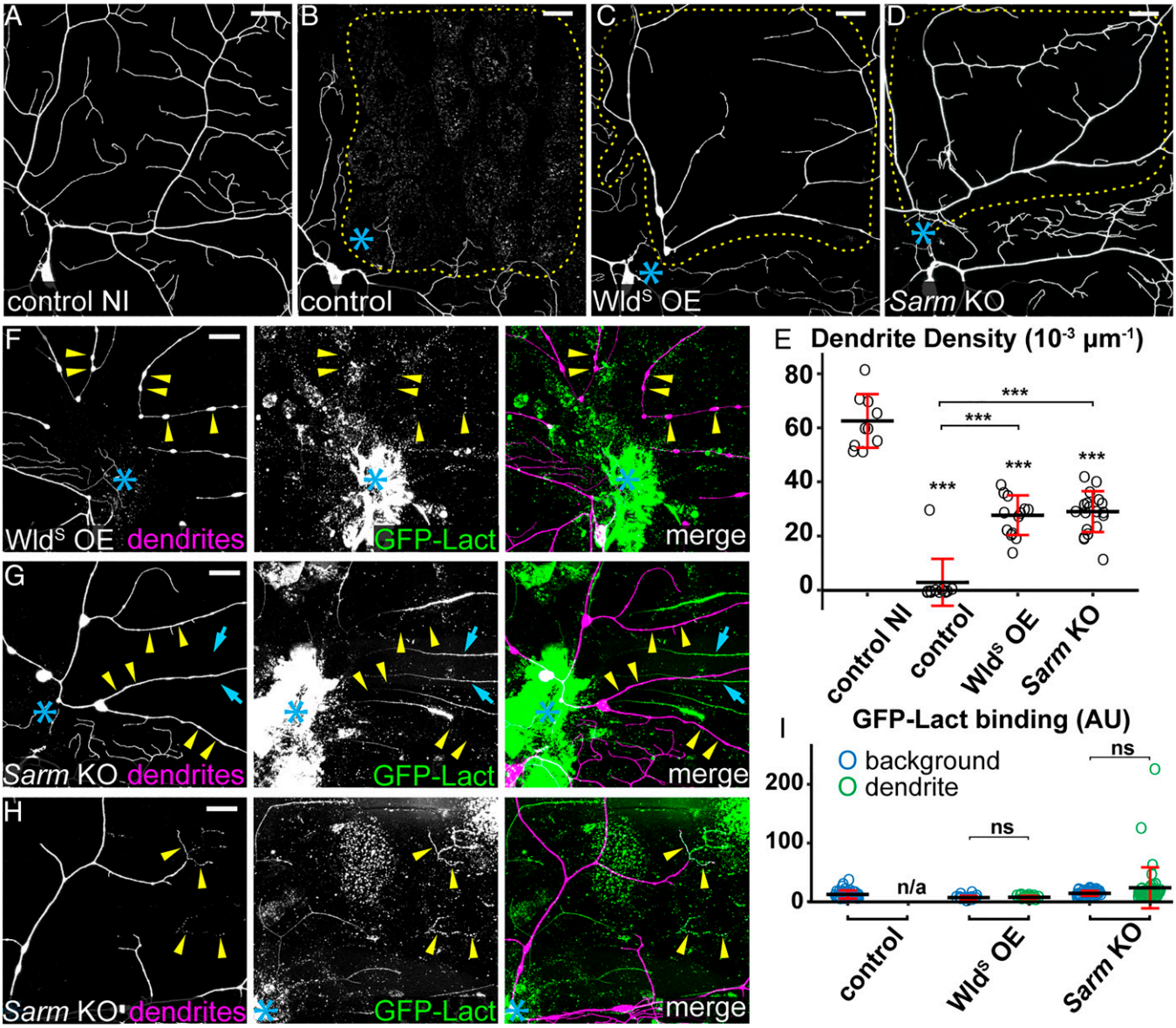

Fig. 3. Wld^S OE and *Sarm* KO suppress PS exposure and fragmentation of injured dendrites. (*A*) Partial dendritic field of an uninjured ddaC control neuron. (*B–D*) Partial dendritic fields of control (*B*), Wld^S OE (*C*), and *Sarm* KO (*D*) ddaC neurons 24 h AI. Blue asterisk, injury site. Yellow dots outline regions covered by injured dendrites. (*E*) Quantification of dendrite density (1,000 × dendritic length/area) in regions covered by injured dendrites. *n* = number of neurons: control no injury (NI) (*n* = 10, 10 animals); control (*n* = 12, six animals); Wld^S OE (*n* = 13, six animals); and *Sarm* KO (*n* = 19, six animals). (*F* and *G*) Wld^S OE (*F*) and *Sarm* KO (*G*) ddaC neurons 24 h AI, showing unfragmented dendrites and the lack of GFP-Lact binding on severed dendrites (yellow arrowheads) of ddaC neurons. GFP signals that do not colocalize with tdTom signals are likely GFP-Lact binding to injured non-C4da neurons without *Sarm* KO (cyan arrows). (*H*) Dendrites of a *Sarm* KO ddaC neuron 24 h AI, showing infrequent GFP-Lact binding at fragmented terminal branches (yellow arrowheads). (*I*) Quantification of GFP-Lact binding on injured dendrites. The GFP-Lact intensity is shown for both background epidermal regions and injured dendrites. The outliers in *Sarm* KO dendrite dataset correspond to infrequent degenerating terminal branches. Background: epidermal regions without dendrites. *n* = number of measurements: control background (*n* = 39) and control dendrite (n/a, no remaining dendrites), seven animals; Wld^S OE background (*n* = 18) and Wld^S OE dendrite (*n* = 18), four animals; and *Sarm* KO background (*n* = 48) and *Sarm* KO dendrite (*n* = 48), nine animals. In all panels, neurons were labeled by *ppk-MApHS* (*A–C*; only tdTom channel is shown), *ppk > CD4-tdTom* (*D*), and *ppk-CD4-tdTom* (*F–H*). Neuronal-specific KO was induced by *SOP-Cas9*. For all quantifications, one-way ANOVA and Tukey test, ***$P \leq 0.001$, ns, not significant, and n/a, not applicable. The significance level above each genotype in *E* is for comparison with the control. Black bar, mean; red bar, SD. (Scale bars, 25 µm.)

Because injury induces a more-rapid and stronger PS exposure on dendrites than *CDC50* KO or TMEM16F OE (24), our data strongly suggest that injury-induced PS exposure is a major driver of dendrite breakdown by activating phagocytosis by epidermal cells.

Injury and Sarm Gain of Function Cause Phagocytosis-Independent Dendrite Self-Destruction. Although *drpr* LOF, either in *drpr* mutants (Fig. 5*B*) or epidermis-specific *drpr* KO (*SI Appendix*, Fig. S3*A*), effectively blocked engulfment of injured dendrites of da neurons, these dendrites nevertheless fragmented by 24 h AI (Fig. 5 *A–C* and *SI Appendix*, Fig. S3*A*) (30), suggesting that dendrite self-destruction took place in the absence of phagocytosis. A neurite self-destruction program triggered by NAD^+ depletion is thought to drive WD of cultured neurons in the absence of phagocytes (21). To test the possibility that further progression of the WD pathway beyond the point of neuronal PS exposure activates dendrite self-destruction, we examined the effect of overexpressing a

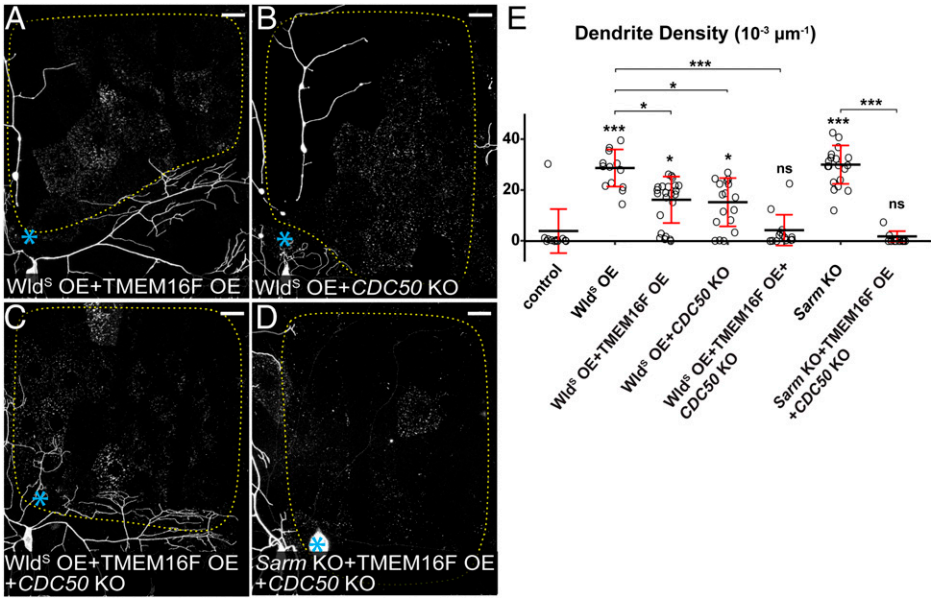

Fig. 4. Ectopic PS exposure causes injured dendrites of Wld^S OE and *Sarm* KO neurons to degenerate. (*A–D*) Partial dendritic fields of Wld^S OE + TMEM16F OE (*A*), Wld^S OE + *CDC50* KO (*B*), Wld^S OE + TMEM16F OE + *CDC50* KO (*C*), and *Sarm* KO + TMEM16F OE + *CDC50* KO (*D*) ddaC neurons 24 h AI. Blue asterisk, injury site. Yellow dots outline regions covered by injured dendrites. Neurons were labeled by *ppk-MApHS* (*A–C*) and *ppk-CD4-tdTom* (*D*). Neuronal-specific KO was induced by *ppk-Cas9* (*B* and *C*) and *SOP-Cas9* (*D*). (Scale bars, 25 µm.) (*E*) Quantification of dendrite density. *n* = number of neurons: control (*n* = 12, six animals); Wld^S OE (*n* = 13, six animals); Wld^S OE + TMEM16F OE (*n* = 23, eight animals); Wld^S OE + *CDC50* KO (*n* = 17, eight animals); Wld^S OE + TMEM16F OE + *CDC50* KO (*n* = 16, eight animals); *Sarm* KO (*n* = 19, six animals); and *Sarm* KO + TMEM16F OE + *CDC50* KO (*n* = 13, seven animals) (Kruskal–Wallis (one-way ANOVA on ranks) and Dunn's test). *P* values were adjusted with the Benjamini–Hochberg method. The dataset for Wld^S OE and *Sarm* KO is the same as in Fig. 3*E*. For all quantifications, $*P \leq 0.05$, $***P \leq 0.001$, and ns, not significant. The significance level above each genotype is for comparison with the control. Black bar, mean; red bar, SD.

gain-of-function (GOF) Sarm (Sarm^{GOF}) in C4da neurons, because Sarm^{GOF} potently depletes NAD$^+$ and causes dominant neurodegeneration (22). Indeed, Sarm^{GOF} OE caused complete dendrite degeneration in most neurons as early as 24 h after egg laying (AEL) (Fig. 5 *D* and *J*), while *Nmnat* KO did not cause dendrite degeneration until 88 to 91 h AEL. Consistent with the role of engulfment in *Nmnat* KO-induced dendrite degeneration, *drpr* LOF strongly suppressed dendrite degeneration of Sarm^{GOF} OE neurons at both 24 h AEL and 48 h AEL (Fig. 5 *E*, *G*, and *J*). However, *drpr* LOF failed to prevent dendrite fragmentation of Sarm^{GOF} OE neurons at wandering third instar (Fig. 5 *H–J*), suggesting that Sarm GOF is able to cause phagocytosis-independent dendrite self-destruction. These results together support the hypothesis that dendrite self-destruction activated by the WD pathway, likely through NAD$^+$ depletion, is responsible for the fragmentation of injured dendrites when phagocytosis is suppressed.

Axed Promotes Self-Destruction of Injured Dendrites in Parallel with Drpr-Dependent Phagocytosis. To understand how other components of the WD pathway regulate dendrite degeneration, we examined *axed* and *peb*, whose roles in da neurons have not been explored. We first confirmed the effectiveness of tissue-specific KO of *axed* in Or22a olfactory neurons (29), which showed effective suppression of WD of severed axons (*SI Appendix*, Fig. S4 *A–D* and *G*), consistent with the previous report (22). We then validated the role of Axed in WD of C4da axons: both KO and knockdown of *axed* efficiently blocked injury-induced axon degeneration (*SI Appendix*, Fig. S4 *H–K*). To determine if Axed is involved in dendrite degeneration, we first tested its role in PS exposure-induced dendrite degeneration of *Nmnat* KO neurons. Unlike *Sarm* KO, which fully rescued *Nmnat* KO-induced degeneration (*SI Appendix*, Fig. S4 *M*, *O*, *P*, and *Q*), *axed* KO did not affect dendrite degeneration caused by *Nmant* KO (*SI Appendix*, Fig. S4 *L*, *N*, *P*, and *Q*), suggesting that *axed* is not required for the PS exposure downstream of *Nmnat* loss and Sarm activation.

We next asked whether Axed is involved in injury-induced dendrite degeneration. Injured dendrites of wild-type neurons completely fragmented by 10 h AI (Fig. 6 *A* and *E*). *axed* KO in neurons resulted in incomplete and no fragmentation of injured dendrites only in small fractions (25% and 8%, respectively) of neurons (Fig. 6 *B* and *E*), suggesting that *axed* is not absolutely required for the degeneration of injured dendrites. Because phagocytosis and self-destruction are each sufficient to break down injured dendrites, we next asked whether Axed specifically contributes to self-destruction of injured dendrites by examining the effect of *axed* KO in *drpr* mutant. *drpr* LOF alone caused incomplete and no dendrite fragmentation in 36% and 23% injured neurons, respectively (Fig. 6 *C* and *E*), consistent with the idea that phagocytosis contributes significantly to dendrite breakdown at this stage. In comparison, *axed* KO in *drpr* mutant strongly blocked dendrite degeneration at 10 h AI, with 56% incomplete fragmentation and 36% no fragmentation (Fig. 6 *D* and *E*), suggesting that *axed* KO and *drpr* LOF have an additive effect in dendrite protection. Surprisingly, this combined protection was significantly weakened by 24 h AI, with only 47% incomplete fragmentation and 5% no fragmentation (Fig. 6 *F–J*). These data suggest that Axed promotes dendrite self-destruction in parallel with phagocytosis; however, other factors can also cause self-destruction in the absence of Axed.

In contrast to *axed*, *peb* KO in C4da neurons did not block dendrite fragmentation AI but altered dendrite morphology (*SI Appendix*, Fig. S4 *R–T*). To validate the role of *peb* in axon degeneration of Or22a neurons, we knocked it out from precursors of olfactory neurons. Unexpectedly, this caused the loss of some or all of Or22a axons in uninjured adult brains (*SI Appendix*, Fig. S4*G*), suggesting that *peb* plays a role in Or22a development or axon patterning. The remaining axons of *peb* KO neurons did not show defects in axon degeneration AI

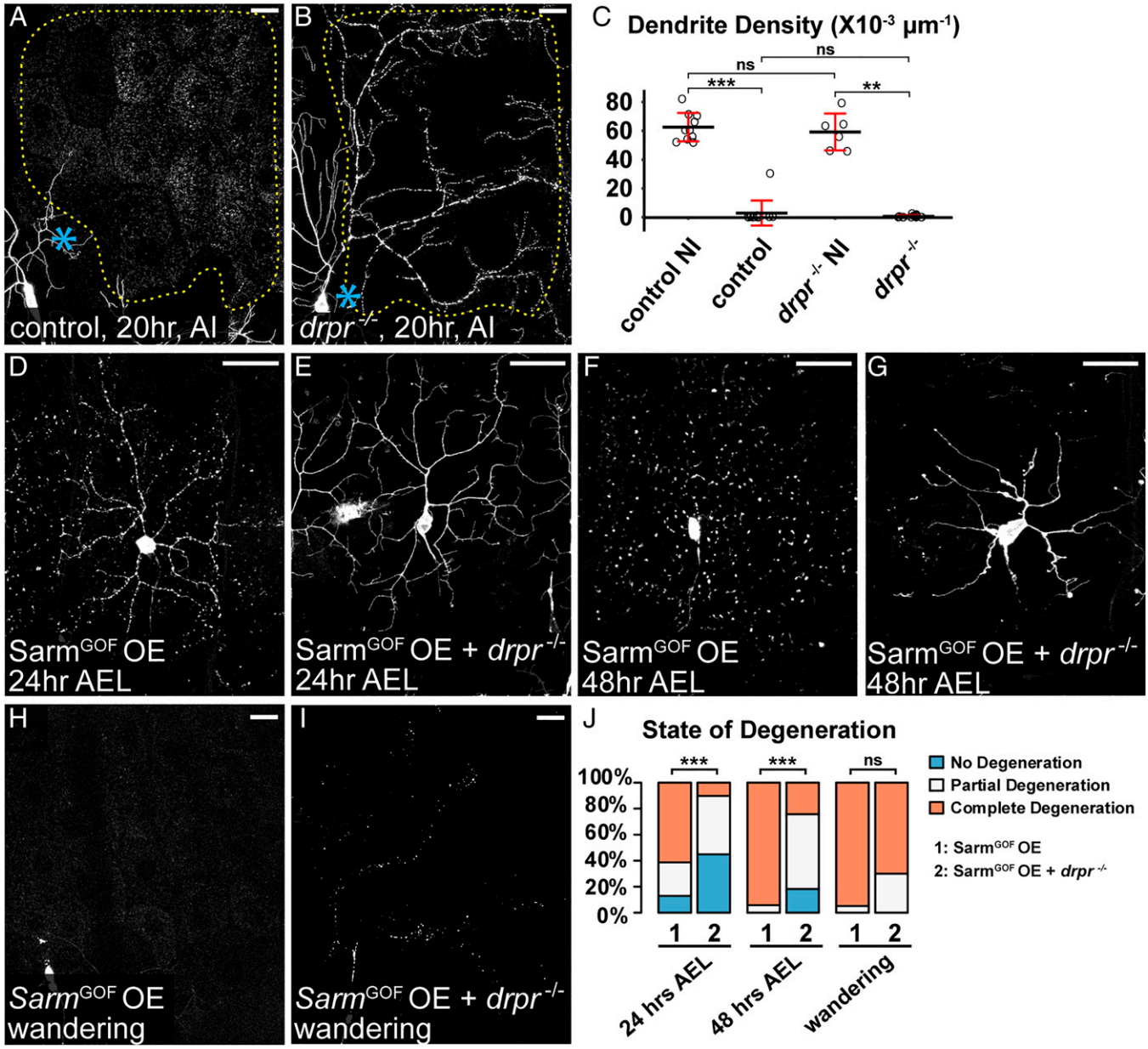

Fig. 5. Injury and Sarm GOF cause phagocytosis-independent dendrite self-destruction. (*A* and *B*) Partial dendritic fields of ddaC neurons in control (*A*) and $drpr^{-/-}$ (*B*) animals 20 h AI. The dendrite debris lining up in the original dendritic pattern in *B* indicates dendrite fragmentation and the lack of epidermal engulfment. Blue asterisk, injury site. Yellow dots outline regions covered by injured dendrites. (*C*) Quantification of dendrite density. *n* = number of neurons: control no injury (NI) (*n* = 10, 10 animals); control AI (*n* = 12, six animals); $drpr^{-/-}$ NI (*n* = 6, five animals); $drpr^{-/-}$ AI (*n* = 13, five animals) (Kruskal–Wallis, one-way ANOVA on ranks, and Dunn's test). *P* values were adjusted with the Benjamini–Hochberg method. (*D–G*) ddaC neurons in $Sarm^{GOF}$ OE 24 h AEL (*D*), $Sarm^{GOF}$ OE + $drpr^{-/-}$ 24 h AEL (*E*), $Sarm^{GOF}$ OE 48 h AEL (*F*), and $Sarm^{GOF}$ OE + $drpr^{-/-}$ 48 h AEL (*G*). (*H–I*) Partial dendritic fields of $Sarm^{GOF}$ OE (*H*) and $Sarm^{GOF}$ OE + $drpr^{-/-}$ (*I*) ddaC neurons at the wandering stage. (*J*) Quantification of dendrite degeneration showing percentages of neurons undergoing partial degeneration, complete degeneration, and no degeneration. *n* = number of neurons: $Sarm^{GOF}$ OE 24 h AEL (*n* = 31, seven animals); $Sarm^{GOF}$ OE + $drpr^{-/-}$ 24 h AEL (*n* = 49, 17 animals); $Sarm^{GOF}$ OE 48 h AEL (*n* = 17, seven animals); $Sarm^{GOF}$ OE + $drpr^{-/-}$ 48 h AEL (*n* = 33, 11 animals); $Sarm^{GOF}$ OE wandering (*n* = 19, 14 animals); and $Sarm^{GOF}$ OE + $drpr^{-/-}$ wandering (*n* = 10, six animals) (Freeman–Halton extension of Fisher's exact test). In image panels above, neurons were labeled by *ppk-MApHS* (*A* and *B*) and *ppk* > *CD4-tdTom* (*D–I*). C4da-specific KO was induced by *ppk-Cas9*. For all quantifications, $^{**}P \leq 0.01$, $^{***}P \leq 0.001$, and ns, not significant. Black bar, mean; red bar, SD. (Scale bars, 25 µm.)

(*SI Appendix*, Fig. S4 *E–G*). These results suggest that Peb may be a neuronal, type-specific modulator of the WD pathway and is not required for dendrite degeneration of da neurons.

Injured Dendrites Undergo Severe Membrane Rupture during Dendrite Fragmentation. Compared to *Nmnat* KO, which causes dendrite degeneration through PS-mediated phagocytosis, injury additionally activates self-destruction. To further understand how injury causes dendrite degeneration, we investigated the extent of membrane rupture during dendrite breakdown using a split GFP-based assay. In this membrane-rupture assay (Fig. 7*A*), neurons express myristoylated tdTom-GFP(1-10), and the fat body secretes $GFP(11)_{x7}$ into the hemolymph. $GFP(11)_{x7}$ will bind myr-tdTom-GFP(1-10) and reconstitute fluorescent GFP only when the dendrite membrane is ruptured to allow diffusion of $GFP(11)_{x7}$ into the cytoplasm of neurons. As expected, we could not detect reconstituted GFP in uninjured neurons (Fig. 7*F*) or intact dendrites of injured neurons

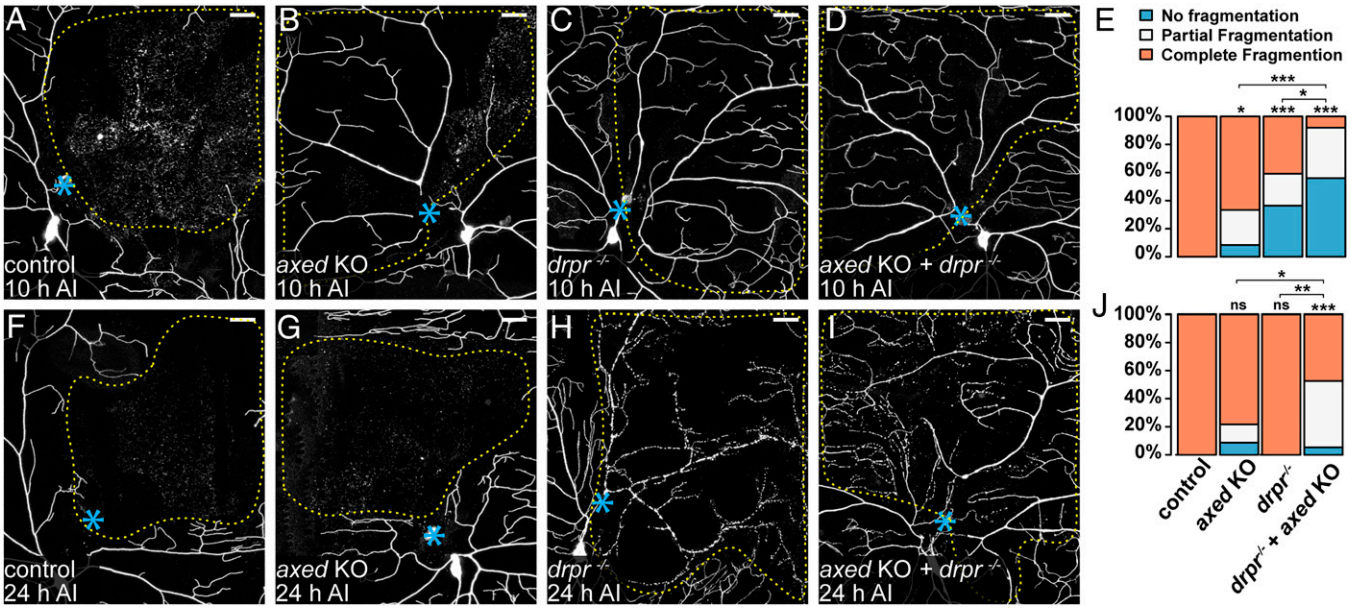

Fig. 6. Axed promotes self-destruction of injured dendrites in parallel with Drpr-dependent phagocytosis. (*A–D*) Partial dendritic fields of wild-type (*A*), *axed* KO (*B*), $drpr^{-/-}$ (*C*), and *axed* KO + $drpr^{-/-}$ (*D*) ddaC neurons 10 h AI. *B* shows partial fragmentation; *C* and *D* show no fragmentation. (*E*) Quantification of dendrite fragmentation showing percentages of neurons undergoing no fragmentation, partial fragmentation, and complete fragmentation of injured dendrites at 10 h AI. *n* = number of neurons: wild-type (*n* = 18, nine animals); *axed* KO (*n* = 24, 10 animals); $drpr^{-/-}$ (*n* = 22, 11 animals); and *axed* KO + $drpr^{-/-}$ (*n* = 25, 11 animals) (Freeman–Halton extension of Fisher's exact test). (*F–I*) Partial dendritic fields of wild-type (*F*), *axed* KO (*G*), $drpr^{-/-}$ (*H*), and *axed* KO + $drpr^{-/-}$ (*I*) ddaC neurons 24 h AI. *I* shows partial fragmentation. In all image panels, blue asterisks indicate injury sites; yellow dots outline regions covered by injured dendrites. Neurons were labeled by *ppk* > *CD4-tdTom* (*A*, *B*, *F*, and *G*) and *ppk-CD4-tdTom* (*C*, *D*, *H*, and *I*). Neuronal-specific KO was induced by *SOP-Cas9* (*B*, *D*, *G*, and *I*). (Scale bars, 25 μm.) (*J*) Quantification of dendrite fragmentation showing percentages of neurons undergoing no fragmentation, partial fragmentation, and complete fragmentation of injured dendrites at 24 h AI. *n* = number of neurons: wild-type (*n* = 21, 12 animals); *axed* KO (*n* = 23, 10 animals); $drpr^{-/-}$ (*n* = 12, five animals); and *axed* KO + $drpr^{-/-}$ (*n* = 19, eight animals) (Freeman–Halton extension of Fisher's exact test). For all quantifications, $*P \leq 0.05$, $**P \leq 0.01$, $***P \leq 0.001$, and ns, not significant. The significance level above each genotype is for comparison with the wild-type.

(*SI Appendix*, Fig. S5*A*). Interestingly, GFP signal was also absent from degenerating dendrites (open arrowheads) and the debris (open arrows) of *Nmnat* KO neurons (Fig. 7 *B*, *E*, and *F*). In contrast, GFP signals were observed in severed wild-type dendrites that were undergoing fragmentation (Fig. 7 *D* arrowheads and *F*) as well as on large membrane pieces shed from injured dendrites (Fig. 7 *D* arrows and *E*). The same dendrite branches showed no GFP signals prior to fragmentation (Fig. 7*C*), suggesting that injured dendrites undergo severe membrane rupture only during fragmentation. These results suggest that compared to injured dendrites, *Nmnat* KO dendrites experience much-milder disruptions of membrane integrity, even though they are losing membranes due to the attack of epidermal cells.

Injured Dendrites Exhibit Calcium-Flashing That Is Suppressed by Wld^S and *axed* Loss. Dendrite injuries cause PS exposure and membrane rupture. To understand potential signaling pathways that may lead to these events, we examined calcium dynamics in injured dendrites using long-term time-lapse imaging (46, 47), because calcium influx is essential for and correlates with degeneration of damaged axons in neuronal culture and in vivo (48–50). A previous study in zebrafish identified an initial calcium influx at the time of axon-severing and a second calcium wave that coincides with axon fragmentation (48). We recorded calcium dynamics using a membrane-tethered GCaMP6s (myr-GCaMP6s) (51), which detected only occasional local rise of calcium in dendrites of wild-type (Movie S3) and *Nmnat* KO neurons (Movie S4). In the injury model, we observed an initial calcium rise immediately after laser injury in both detached dendrites and the rest of the neurons (Fig. 8*A*, 2 s AI). Interestingly, soon after calcium dropped to the baseline level, severed dendrites but not those connected to the cell body entered a phase of continuous calcium flashes that lasted 1 to 5 h (Fig. 8 *A* at 1 h AI and *D*, and Movie S5). Afterward, severed dendrites stayed relatively quiescent for 1 to 3 h before calcium surged again at the time of dendrite blebbing and fragmentation (Fig. 8 *A* at 6 h AI and *D*, and Movie S5). All severed dendrites but not those still attached to cell bodies showed flashing, quiescence, and surge phases AI, even though the exact timing and duration of each phase varied from dendrite to dendrite (*SI Appendix*, Fig. S6 *A* and *D*).

It was reported that nanoscale ruptures of the axonal plasma membrane are responsible for extracellular calcium influx in neuroinflammatory lesions (52) and after spinal cord contusion (50). To determine whether the last calcium rise that coincides with dendrite fragmentation could be a result of phagocytosis-induced membrane breakage, we imaged both calcium dynamics and PS exposure of injured dendrites using the PS sensor Annexin V-mCardinal (AV-mCard) (24). AV-mCard labeling of dendrites appeared slightly ahead of the final calcium surge (Fig. 8 *B* and *C* and Movie S6). Considering that Annexin V binding to PS and accumulation on dendrite surface are likely slower than calcium activation of GCaMP6s, our data suggest that PS exposure on injured dendrites precedes the final calcium surge.

Because the unique pattern of calcium-flashing is absent in uninjured dendrites and *Nmnat* KO neurons, we suspected that it may play an active role in promoting degeneration of injured dendrites. If so, factors that can block dendrite degeneration may also alter the calcium-flashing. Indeed, Wld^S OE dramatically reduced calcium fluctuations in injured dendrites and eliminated the quiescent and surge phases for the entire duration of our time-lapse imaging (13 h) (Fig. 8 *E* and *J*,

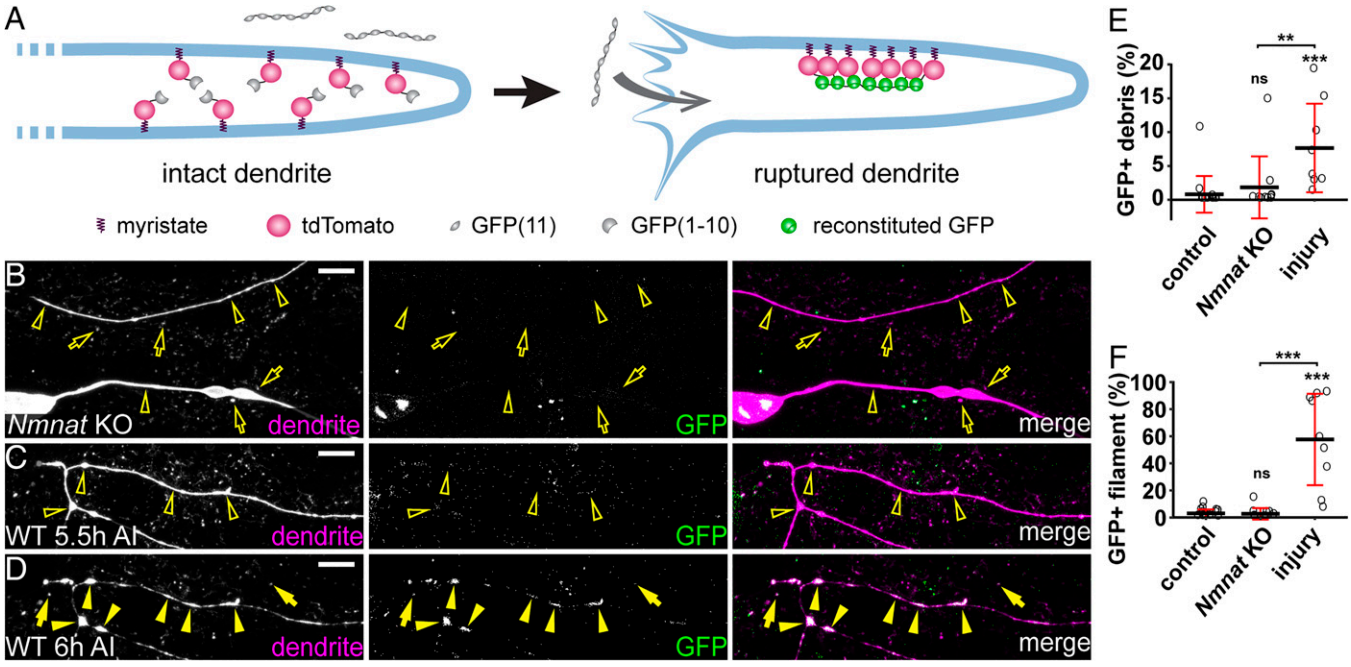

Fig. 7. Injured dendrites undergo severe membrane rupture during dendrite fragmentation. (*A*) A diagram for the membrane-rupture assay. Extracellular $GFP(11)_{x7}$ is separated from intracellular myr-tdTom-GFP(1-10) attached to the inner membrane of dendrites. Fluorescent GFP is reconstituted only when the dendrite membrane is ruptured to allow diffusion of $GFP(11)_{x7}$ into the cytoplasm of neurons. (*B*) *Nmnat* KO dendrites (open arrowheads) and debris (open arrows) lacking reconstituted GFP in the membrane-rupture assay. (Scale bar, 10 μm.) (*C*) Injured wild-type dendrites before fragmentation (open arrowheads) lacking reconstituted GFP at 5.5 h AI. (Scale bar, 10 μm.) (*D*) Reconstituted GFP-labeling in fragmented dendrites (arrowheads) and debris (arrows) at 6 h AI. *C* and *D* show the same dendrites at two different time points. (Scale bar, 10 μm.) (*E*) Quantification of GFP-positive debris, showing the percentage of GFP-positive debris area in tdTom-positive debris area. Number of regions of interests (ROIs): wild-type NI control (n = 15, seven animals); *Nmnat* KO NI (n = 10, six animals); and wild-type 6 h AI (n = 10, four animals). (Kruskal–Wallis, one-way ANOVA on ranks, and Dunn's test). *P* values were adjusted with the Benjamini–Hochberg method. (*F*) Quantification of GFP-positive filament, showing the percentage of GFP-positive filament area in tdTom-positive filament area. Number of ROIs: same as in *D* (Kruskal–Wallis, one-way ANOVA on ranks, and Dunn's test). *P* values were adjusted with the Benjamini–Hochberg method. For all quantifications, $^{**}P \leq 0.01$; $^{***}P \leq 0.001$, and ns, not significant. The significance level above each genotype is for comparison with the control. Black bar, mean; red bar, SD.

SI Appendix, Fig. S6*B*, and Movie S7). In addition, using time-lapse imaging at a higher temporal resolution (2 s/frame), we found that wild-type–injured dendrites displayed calcium flashes at a frequency of 0.4 to 3/min (Fig. 8 *G* and *K* and Movie S8), while injured dendrites of Wld^S OE neurons either maintained a much-milder calcium fluctuation or exhibited irregular and infrequent calcium flashes (Fig. 8 *H*, *K*, and *L* and Movies S9 and S10). In contrast, the majority of severed dendrites of *axed* KO neurons (6/9) maintained constant and high calcium levels before the quiescence and surge phases (Fig. 8 *F* and *J*, *SI Appendix*, Fig. S6*C*, and Movie S11), which was further confirmed by time-lapse imaging at the high temporal resolution (Fig. 8 *I*, *K*, and *L* and Movie S12). Overall, injured dendrites of Wld^S OE and *axed* KO neurons showed much smaller average amplitudes of calcium fluctuations compared to the wild-type control (Fig. 8*L*). Because Wld^S OE and *axed* KO did not alter calcium dynamics in uninjured dendrites (*SI Appendix*, Fig. S6 *E* and *F*), these data suggest that these manipulations specifically modify calcium-flashing patterns in injured dendrites, consistent with the idea that calcium flashes may promote degeneration of injured dendrites.

Discussion

In this study, we investigate mechanisms of dendrite degenerations caused by injury and genetic activation of the WD pathway in the *Drosophila* PNS. Although neurite phagocytosis has been observed after neuronal injury both in vivo and in vitro (24, 29, 30, 53), WD is generally considered as a result of neurite self-destruction triggered by NAD^+ depletion (7, 9, 21, 22). However, our results using engulfment-deficient *drpr* LOF strongly suggest that PS-mediated phagocytosis is the main driving force for WD-related dendrite degeneration in vivo. It is solely responsible for dendrite degeneration of *Nmnat* KO neurons and greatly accelerates the degeneration of $Sarm^{GOF}$ OE neurons. In injury, phagocytosis is responsible for at least half of the dendrite fragmentation by 10 h AI and may contribute more to dendrite breakdown than self-destruction at earlier stages. Supporting this idea, ectopic PS exposure on injured dendrites is sufficient to revert the blockage of dendrite fragmentation by Wld^S OE or *Sarm* KO, even though ectopically induced PS exposure is much lower than natural PS exposure on injured dendrites (24). Our time-lapse analyses of PS exposure, the final calcium surge, and dendrite rupture also support the possibility that PS-mediated phagocytosis breaks down injured dendrites at the time of dendrite fragmentation. Therefore, at least in the context of dendrite injury, phagocytosis is the major factor driving WD, while self-destruction acts as a secondary mechanism to ensure complete fragmentation.

NAD^+ reduction is thought to be responsible for neuronal PS exposure and neurite self-destruction during WD (21, 24, 32). How may NAD^+ reductions coordinate the two different events? Our results support a hypothesis that NAD^+ disruption controls PS exposure and neurite self-destruction in two separate steps of WD. In the existing model, Sarm activation is believed to cause catastrophic NAD^+ depletion that is sufficient to initiate neurite self-destruction (11, 21). However, we found that downstream of Sarm activation and before the initiation of self-destruction, neurites first expose PS to engage in phagocytosis-mediated nonautonomous degeneration. Therefore, in our revised model, dendrites

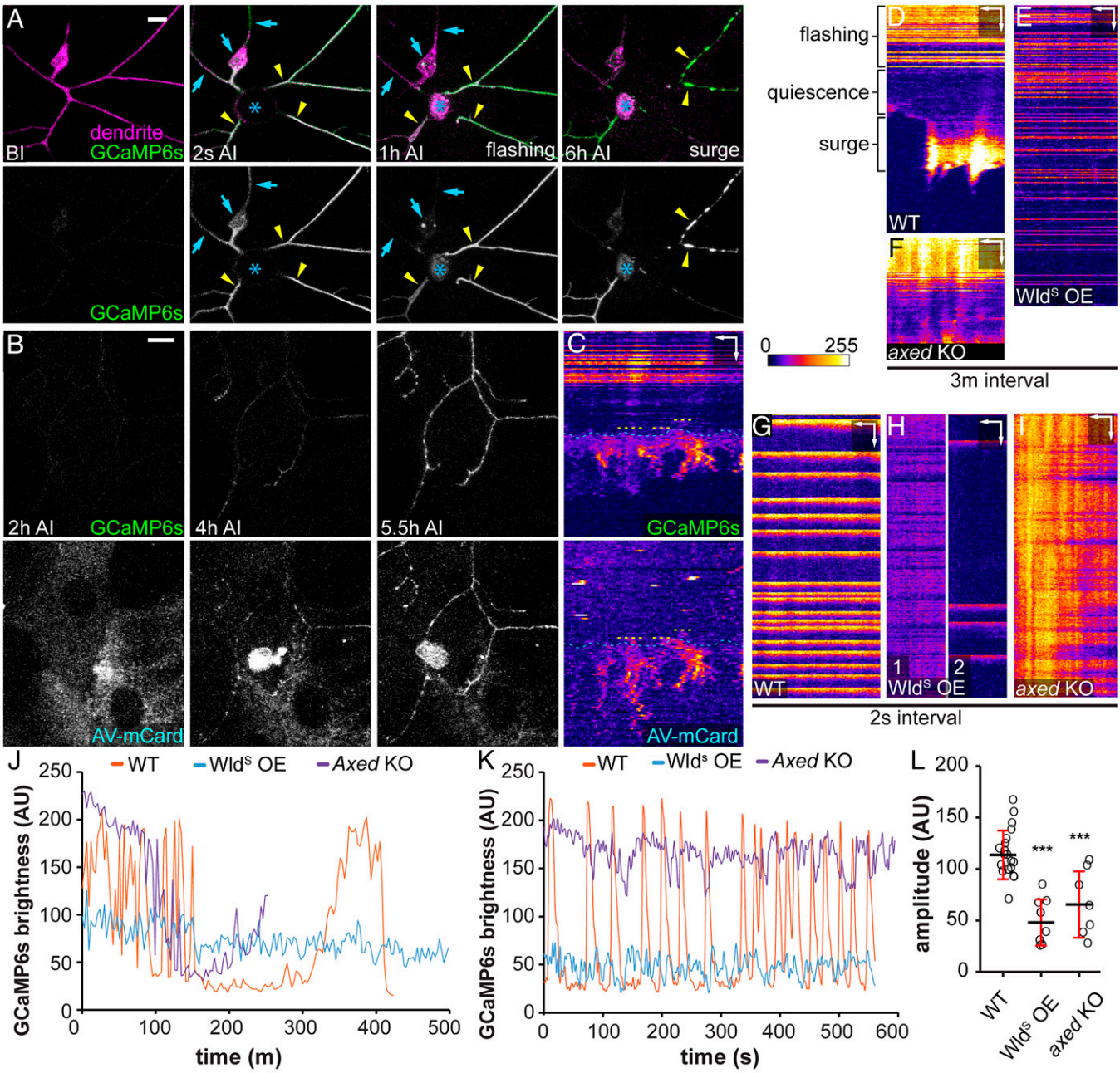

Fig. 8. Injured dendrites exhibit calcium-flashing that is suppressed by Wld^S and *axed* loss. (*A*) A ddaC neuron in a third instar larva expressing myr-GCaMP6s before (BI) and after (2 s AI, 1 h AI, and 6 h AI) laser injury. Blue arrows, uninjured dendrites or cell body; yellow arrowheads, injured dendrites; and blue asterisk, injury site. (Scale bar, 10 μm) (Movie S5). (*B*) Labeling of injured ddaC dendrites expressing GCaMP6s by AV-mCard after (2, 4, and 5.5 h) injury. (Scale bar, 10 μm.) (Movie S6). (*C*) Kymograph of GCaMP6s signal and AV-mCard binding on an injured dendrite shown in *B*. Yellow dotted lines, timing of AV-mCard binding; blue dotted lines, timing of the final calcium surge. (Scale bars, 3 μm horizontal, 40 min vertical.) (*D–F*) Kymograph of GCaMP6s signal in wild-type (*D*), Wld^S-overexpressing (*E*), and *axed* KO (*F*) dendrites AI with 3-min interval (Movies S5, S7, and S11). (Scale bar, 5 μm horizontal, 60 min vertical.) (*G–I*) Kymograph of GCaMP6s signal in wild-type (*G*), Wld^S-overexpressing (*H*), and *axed* KO (*I*) dendrites AI with 2-s interval (Movies S8, S9, S10, and S12). (Scale bars, 5 μm horizontal, 45 s vertical.) (*J*) Plot of GCaMP6s brightness in injured dendrites in *D–F* over time with 3-m interval. Measurements in injured dendrites start from 0.5 to 1 h AI. (*K*) Plot of GCaMP6s brightness in injured dendrite in *G–I* over time with 2-s interval. Measurements start from 0.5 to 1 h AI. (*L*) Quantification of average flashing amplitude (GCaMP6s brightness difference between maximum peak and neighboring minimum peak) captured in 2-s interval time-lapse images. N = number of dendrite arbors: wild-type 0.5 to 1.5 h AI (n = 19, five animals); Wld^S-overexpressing 2 h AI (n = 8, four animals); and *axed* KO 0.5 to 1 h AI (n = 7, three animals) (one-way ANOVA and Tukey's test). For all quantifications, $^{***}P \leq 0.001$ and ns, not significant. The significance level above each genotype is for comparison with the control. Black bar, mean; red bar, SD.

respond to at least three distinct, increasingly severe levels of NAD$^+$ reduction by eliciting different molecular events (*SI Appendix*, Fig. S7). Between the NAD$^+$ level required for Sarm activation (SA level) and the level that initiates self-destruction (the self-destruction level), Sarm activity lowers NAD$^+$ to a level that causes neurons to expose PS on their surface (which we call the PSE level). This PS exposure is sufficient to cause phagocytosis-mediated dendrite degeneration, which can be completely prevented by blocking engulfment activity of phagocytes. However, below the self-destruction level,

neurites spontaneously fragment even in the absence of phagocytosis.

This model is consistent with an apparent correlation between the expected kinetics of NAD^+ reduction and the severity of neurite degeneration. *Nmnat* KO is expected to cause slow NAD^+ reduction, due to gene perdurance and the time required for natural NAD^+ turnover, and correspondingly causes engulfment-dependent dendrite degeneration only in late third instar larvae. In contrast, $Sarm^{GOF}$ OE should lead to a more-rapid NAD^+ depletion and in fact causes engulfment-dependent dendrite degeneration as early as the first instar and dendrite self-destruction by the third instar. Injury is known to cause even more rapid NAD^+ reduction in axons (20) and is correlated with the fastest dendrite degeneration—initiation at around 4 h AI and completion usually by 10 h AI. Directly validating this model will likely require a sensitive NAD^+ indicator that can measure NAD^+ levels in dendrites in vivo.

How may NAD^+ reduction cause PS exposure? A direct consequence of NAD^+ loss is the decline of neurite ATP levels due to the requirement of NAD^+ in glycolysis and oxidative phosphorylation (20, 32). Consistent with ATP reduction playing a role in inducing PS exposure, suppressing mitochondria ATP synthesis in dorsal root ganglia (DRG) culture caused gradual axonal PS exposure (32). However, how ATP reduction may induce PS exposure remains elusive. Although the maintenance of membrane PS asymmetry by flippases requires ATP, flippase KO in C4da neurons causes a much-milder PS exposure than injury (24), suggesting that mechanisms other than flippase inhibition must be contributing to the rapid PS exposure seen AI. Identifying the PS transporters responsible for PS exposure on injured neurites will be a key step for revealing the mechanisms of NAD^+ regulation of PS exposure.

Genetic analyses in *Drosophila* identified Axed as a key switch of WD, whose activity is absolutely required for axon degeneration caused by injury and Sarm GOF (22). How does Axed regulate neurite degeneration? Our data suggest that Axed is not required for PS-mediated phagocytosis but contributes to the self-destruction of injured dendrites, placing its activation below the self-destruction level of NAD^+ in our model (*SI Appendix*, Fig. S7). Surprisingly, Axed seems to play a minor role in dendrite degeneration, as its LOF only slowed down but did not block self-destruction, indicating the existence of other factors that promote self-destruction of injured dendrites.

By exploring the different mechanisms employed in *Nmnat* KO- and injury-induced dendrite degenerations, we discovered dynamic calcium activities that are only present in injured dendrites, including a calcium-flashing pattern prior to any obvious degenerative event and a final calcium surge that coincides with dendrite fragmentation. Calcium surge at the time of neurite fragmentation is a shared feature between injured axons of zebrafish (48) and injured dendrites of *Drosophila* da neurons. Although calcium influx is required for WD (49) and may activate calcium-dependent lipid scramblases (54), our time-lapse analyses suggest that the final calcium surge is more likely a result of phagocytosis-induced membrane rupture rather than the cause of fragmentation. In comparison, the calcium-flashing soon after the injury is unique to dendrites and may play an active role in dendrite degeneration in ways similar to the compartmentalized calcium-flashing that occurs during developmental pruning of C4da neurons (55). Consistent with this possibility, the calcium-flashing is suppressed by Wld^S OE and *axed* KO. Interestingly, these two manipulations block the calcium-flashing in opposite ways, with Wld^S OE dampening the calcium level and *axed* KO keeping the calcium level high. This distinction may be a useful clue for understanding the regulation of PS exposure and self-destruction. For example, it is possible that elevated calcium levels prepare dendrites for PS exposure and drastic changes of calcium levels promote dendrite self-destruction.

Previous studies have shown that axons and dendrites share common features in neurite degeneration: they both undergo PS exposure and WD AI (24, 32, 33, 56), they are both subject to PS exposure-induced degeneration (24), and injury-induced PS exposure and degeneration of both can be blocked by manipulations to increase NAD^+ levels (24, 32, 40). Our analyses on *Nmnat* and *Sarm* additionally show that dendrites are similar to axons in SARM-dependent spontaneous degeneration associated with *NMNAT* deficiency (42, 57). Unexpectedly, our results also reveal important differences between dendrites and axons. First, while Axed is absolutely required for axon degeneration in injury and in Sarm GOF (22), it is only partially involved in dendrite degeneration AI. Second, calcium-flashing is found in dendrites that are injured or undergoing developmental pruning (55) but not in injured axons (48). These results suggest that dendrites and axons utilize both shared and neurite type-specific programs in degeneration.

Lastly, as impairment of NAD^+ metabolism is a general feature of neurodegenerative disorders including Leber congenital amaurosis, Alzheimer's disease, Parkinson's disease, and retinal degenerations (39, 58–61), phagocytosis may play important roles in the pathogenesis of these diseases through dysregulated neuronal PS exposure.

Methods

Fly Strains. The details of fly strains used in this study are listed in *SI Appendix*, Table S1. For labeling of C4da neurons, we used *ppk-CD4-tdTom*, *ppk-MApHS*, and *ppk-Gal4 UAS-CD4-tdTom*. For labeling of all da neurons, we used *RabX4-Gal4 UAS-MApHS*. For labeling PS exposure on dendrites, we used *dcg-Gal4 UAS-GFP-LactC1C2*, *R16A03-LexA LexAop-GFP-LactC1C2*, and *dcg-Gal4 UAS-AnnexinV-mCard*. To label Or22a axons, we used *Or22a-Gal4 UAS-mCD8-GFP*. To visualize dendrite rupture, we used *dcg-Gal4 UAS-sGFP(11)x7* together with *ppk-LexA LexAop-myr-tdTom-GFP(1-10)*. To visualize calcium activities in C4da dendrites, we used *ppk-LexA LexAop-myr-GCaMP6s*.

Refer to *SI Appendix, SI Methods* for details of molecular cloning and transgenic flies, CRISPR-TRiM, live imaging, image analysis and quantification, and statistical analysis. Refer to *SI Appendix*, Table S2 for gRNA target sequences.

Data Availability. All study data are included in the article and/or supporting information.

ACKNOWLEDGMENTS. We thank Marc Freeman, Yang Xiang, Heather Broihier, and Bloomington Stock Center for fly stocks; Addgene for plasmids; Cornell Biotechnology Resource Center (BRC) Imaging facility for access to microscopes (funded by NIH Grant S10OD018516); Cornell Statistical Consulting Unit (CSCU) for advice on statistics; and Mike Goldberg and Fenghua Hu for critical reading of and suggestions on the manuscript. This work was supported by a Cornell start-up fund and NIH grants (R01NS099125 and R21OD023824) awarded to C.H.

1. A. Waller, Experiments on the section of the glossopharyngeal and hypoglossal nerves of the frog, and observations of the alterations produced thereby in the structure of their primitive fibres. *Philos. Trans. R. Soc. Lond.* **140**, 423–429 (1850).
2. M. P. Coleman, M. R. Freeman, Wallerian degeneration, Wld(s), and Nmnat. *Annu. Rev. Neurosci.* **33**, 245–267 (2010).
3. J. Tao, M. M. Rolls, Dendrites have a rapid program of injury-induced degeneration that is molecularly distinct from developmental pruning. *J. Neurosci.* **31**, 5398–5405 (2011).
4. M. L. Sapar, C. Han, Die in pieces: How *Drosophila* sheds light on neurite degeneration and clearance. *J. Genet. Genomics* **46**, 187–199 (2019).
5. D. A. Galloway, A. E. M. Phillips, D. R. J. Owen, C. S. Moore, Phagocytosis in the brain: Homeostasis and disease. *Front. Immunol.* **10**, 790 (2019).
6. A. J. Davies *et al.*, Natural killer cells degenerate intact sensory afferents following nerve injury. *Cell* **176**, 716–728.e18 (2019).
7. J. Gerdts, D. W. Summers, J. Milbrandt, A. DiAntonio, Axon delf-destruction: New links among SARM1, MAPKs, and NAD+ metabolism. *Neuron* **89**, 449–460 (2016).
8. M. R. Freeman, J. Delrow, J. Kim, E. Johnson, C. Q. Doe, Unwrapping glial biology: Gcm target genes regulating glial development, diversification, and function. *Neuron* **38**, 567–580 (2003).

9. X. Xiong *et al.*, The Highwire ubiquitin ligase promotes axonal degeneration by tuning levels of Nmnat protein. *PLoS Biol.* **10**, e1001440 (2012).
10. E. Babetto, B. Beirowski, E. V. Russler, J. Milbrandt, A. DiAntonio, The Phr1 ubiquitin ligase promotes injury-induced axon self-destruction. *Cell Rep.* **3**, 1422–1429 (2013).
11. R. G. Zhai, M. Rizzi, S. Garavaglia, Nicotinamide/nicotinic acid mononucleotide adenylyltransferase, new insights into an ancient enzyme. *Cell. Mol. Life Sci.* **66**, 2805–2818 (2009).
12. Y. Sasaki, T. Nakagawa, X. Mao, A. DiAntonio, J. Milbrandt, NMNAT1 inhibits axon degeneration via blockade of SARM1-mediated NAD^+ depletion. *eLife* **5**, e19749 (2016).
13. M. Di Stefano *et al.*, A rise in NAD precursor nicotinamide mononucleotide (NMN) after injury promotes axon degeneration. *Cell Death Differ.* **22**, 731–742 (2015).
14. H. W. Liu *et al.*, Pharmacological bypass of NAD^+ salvage pathway protects neurons from chemotherapy-induced degeneration. *Proc. Natl. Acad. Sci. U.S.A.* **115**, 10654–10659 (2018).
15. J. M. Osterloh *et al.*, dSarm/Sarm1 is required for activation of an injury-induced axon death pathway. *Science* **337**, 481–484 (2012).
16. M. Bratkowski *et al.*, Structural and mechanistic regulation of the pro-degenerative NAD hydrolase SARM1. *Cell Rep.* **32**, 107999 (2020).
17. Y. Jiang *et al.*, The NAD^+-mediated self-inhibition mechanism of pro-neurodegenerative SARM1. *Nature* **588**, 658–663 (2020).
18. M. D. Figley *et al.*, SARM1 is a metabolic sensor activated by an increased NMN/NAD^+ ratio to trigger axon degeneration. *Neuron* **109**, 1118–1136.e11 (2021).
19. C. Shen *et al.*, Multiple domain interfaces mediate SARM1 autoinhibition. *Proc. Natl. Acad. Sci. U.S.A.* **118**, e2023151118 (2021).
20. M. Sporny *et al.*, Structural basis for SARM1 inhibition and activation under energetic stress. *eLife* **9**, e62021 (2020).
21. J. Wang *et al.*, A local mechanism mediates NAD-dependent protection of axon degeneration. *J. Cell Biol.* **170**, 349–355 (2005).
22. J. Gerdts, E. J. Brace, Y. Sasaki, A. DiAntonio, J. Milbrandt, SARM1 activation triggers axon degeneration locally via NAD^+ destruction. *Science* **348**, 453–457 (2015).
23. L. J. Neukomm *et al.*, Axon death pathways converge on axundead to promote functional and structural axon disassembly. *Neuron* **95**, 78–91.e5 (2017).
24. J. E. Farley *et al.*, Transcription factor Pebbled/RREB1 regulates injury-induced axon degeneration. *Proc. Natl. Acad. Sci. U.S.A.* **115**, 1358–1363 (2018).
25. M. L. Sapar *et al.*, Phosphatidylserine externalization results from and causes neurite degeneration in *Drosophila*. *Cell Rep.* **24**, 2273–2286 (2018).
26. P. A. Leventis, S. Grinstein, The distribution and function of phosphatidylserine in cellular membranes. *Annu. Rev. Biophys.* **39**, 407–427 (2010).
27. L. Fourgeaud *et al.*, TAM receptors regulate multiple features of microglial physiology. *Nature* **532**, 240–244 (2016).
28. E. F. Nandrot *et al.*, Essential role for MFG-E8 as ligand for alphavbeta5 integrin in diurnal retinal phagocytosis. *Proc. Natl. Acad. Sci. U.S.A.* **104**, 12005–12010 (2007).
29. F. Mazaheri *et al.*, Distinct roles for BAI1 and TIM-4 in the engulfment of dying neurons by microglia. *Nat. Commun.* **5**, 4046 (2014).
30. J. M. MacDonald *et al.*, The *Drosophila* cell corpse engulfment receptor Draper mediates glial clearance of severed axons. *Neuron* **50**, 869–881 (2006).
31. C. Han *et al.*, Epidermal cells are the primary phagocytes in the fragmentation and clearance of degenerating dendrites in *Drosophila*. *Neuron* **81**, 544–560 (2014).
32. T. T. Tung *et al.*, Phosphatidylserine recognition and induction of apoptotic cell clearance by *Drosophila* engulfment receptor Draper. *J. Biochem.* **153**, 483–491 (2013).
33. V. Shacham-Silverberg *et al.*, Phosphatidylserine is a marker for axonal debris engulfment but its exposure can be decoupled from degeneration. *Cell Death Dis.* **9**, 1116 (2018).
34. C. Sievers, N. Platt, V. H. Perry, M. P. Coleman, L. Conforti, Neurites undergoing Wallerian degeneration show an apoptotic-like process with Annexin V positive staining and loss of mitochondrial membrane potential. *Neurosci. Res.* **46**, 161–169 (2003).
35. T. G. Mack *et al.*, Wallerian degeneration of injured axons and synapses is delayed by a Ube4b/Nmnat chimeric gene. *Nat. Neurosci.* **4**, 1199–1206 (2001).
36. R. G. Zhai *et al.*, *Drosophila* NMNAT maintains neural integrity independent of its NAD synthesis activity. *PLoS Biol.* **4**, e416 (2006).
37. Y. Wen, J. Z. Parrish, R. He, R. G. Zhai, M. D. Kim, Nmnat exerts neuroprotective effects in dendrites and axons. *Mol. Cell. Neurosci.* **48**, 1–8 (2011).
38. A. R. Poe *et al.*, Robust CRISPR/Cas9-mediated tissue-specific mutagenesis reveals gene redundancy and perdurance in *Drosophila*. *Genetics* **211**, 459–472 (2019).
39. C. Han, L. Y. Jan, Y. N. Jan, Enhancer-driven membrane markers for analysis of nonautonomous mechanisms reveal neuron-glia interactions in *Drosophila*. *Proc. Natl. Acad. Sci. U.S.A.* **108**, 9673–9678 (2011).
40. Y. O. Ali, D. Li-Kroeger, H. J. Bellen, R. G. Zhai, H. C. Lu, NMNATs, evolutionarily conserved neuronal maintenance factors. *Trends Neurosci.* **36**, 632–640 (2013).
41. M. A. Avery, A. E. Sheehan, K. S. Kerr, J. Wang, M. R. Freeman, Wld^S requires Nmnat1 enzymatic activity and N16-VCP interactions to suppress Wallerian degeneration. *J. Cell Biol.* **184**, 501–513 (2009).
42. J. Gilley, R. Adalbert, G. Yu, M. P. Coleman, Rescue of peripheral and CNS axon defects in mice lacking NMNAT2. *J. Neurosci.* **33**, 13410–13424 (2013).
43. J. Gilley, G. Orsomando, I. Nascimento-Ferreira, M. P. Coleman, Absence of SARM1 rescues development and survival of NMNAT2-deficient axons. *Cell Rep.* **10**, 1974–1981 (2015).
44. K. Tanaka, K. Fujimura-Kamada, T. Yamamoto, Functions of phospholipid flippases. *J. Biochem.* **149**, 131–143 (2011).
45. S. Raiders *et al.*, Glia actively sculpt sensory neurons by controlled phagocytosis to tune animal behavior. *eLife* **10**, e63532 (2021).
46. K. Segawa, J. Suzuki, S. Nagata, Constitutive exposure of phosphatidylserine on viable cells. *Proc. Natl. Acad. Sci. U.S.A.* **108**, 19246–19251 (2011).
47. H. Ji, C. Han, LarvaSPA, a method for mounting *Drosophila* larva for long-term time-lapse imaging. *J. Vis. Exp.* **156**, e60792 (2020).
48. A. R. Poe *et al.*, Dendritic space-filling requires a neuronal type-specific extracellular permissive signal in *Drosophila*. *Proc. Natl. Acad. Sci. U.S.A.* **114**, E8062–E8071 (2017).
49. M. E. Vargas, Y. Yamagishi, M. Tessier-Lavigne, A. Sagasti, Live imaging of calcium dynamics during axon degeneration reveals two functionally distinct phases of calcium influx. *J. Neurosci.* **35**, 15026–15038 (2015).
50. E. B. George, J. D. Glass, J. W. Griffin, Axotomy-induced axonal degeneration is mediated by calcium influx through ion-specific channels. *J. Neurosci.* **15**, 6445–6452 (1995).
51. P. R. Williams *et al.*, A recoverable state of axon injury persists for hours after spinal cord contusion in vivo. *Nat. Commun.* **5**, 5683 (2014).
52. Y. Akbergenova, K. L. Cunningham, Y. V. Zhang, S. Weiss, J. T. Littleton, Characterization of developmental and molecular factors underlying release heterogeneity at *Drosophila* synapses. *eLife* **7**, e38268 (2018).
53. M. E. Witte *et al.*, Calcium influx through plasma-membrane nanoruptures drives axon degeneration in a model of multiple sclerosis. *Neuron* **101**, 615–624.e5 (2019).
54. K. Nomura-Komoike, F. Saitoh, H. Fujieda, Phosphatidylserine recognition and Rac1 activation are required for Müller glia proliferation, gliosis and phagocytosis after retinal injury. *Sci. Rep.* **10**, 1488 (2020).
55. J. Suzuki, M. Umeda, P. J. Sims, S. Nagata, Calcium-dependent phospholipid scrambling by TMEM16F. *Nature* **468**, 834–838 (2010).
56. T. Kanamori *et al.*, Compartmentalized calcium transients trigger dendrite pruning in *Drosophila* sensory neurons. *Science* **340**, 1475–1478 (2013).
57. Y. E. Kim, J. Chen, J. R. Chan, R. Langen, Engineering a polarity-sensitive biosensor for time-lapse imaging of apoptotic processes and degeneration. *Nat. Methods* **7**, 67–73 (2010).
58. J. Gilley, M. P. Coleman, Endogenous Nmnat2 is an essential survival factor for maintenance of healthy axons. *PLoS Biol.* **8**, e1000300 (2010).
59. C. Cantó, K. J. Menzies, J. Auwerx, NAD(+) metabolism and the control of energy homeostasis: A balancing act between mitochondria and the nucleus. *Cell Metab.* **22**, 31–53 (2015).
60. E. F. Fang *et al.*, NAD^+ in aging: Molecular mechanisms and translational implications. *Trends Mol. Med.* **23**, 899–916 (2017).
61. J. B. Lin *et al.*, NAMPT-mediated NAD(+) biosynthesis is essential for vision in mice. *Cell Rep.* **17**, 69–85 (2016).
62. E. Verdin, NAD^+ in aging, metabolism, and neurodegeneration. *Science* **350**, 1208–1213 (2015).